

Suppression of Microbunching Instability in the Linac Coherent Light Source

Z. Huang^a, M. Borland^b, P. Emma^a, J. Wu^a, C. Limborg^a, G. Stupakov^a, J. Welch^a

^aSLAC, Stanford, CA 94309, USA; ^bANL, Argonne, IL 60439, USA

INTRODUCTION

In order to reach the desired electron peak current capable of inducing the collective free-electron laser (FEL) instability in the x-ray regime [1, 2], the pulse length of a low-emittance electron bunch generated from the photocathode rf gun is magnetically compressed in the linear accelerator by more than one order of magnitude. Numerical and theoretical investigations of high-brightness electron bunch compression lead to a coherent synchrotron radiation (CSR) microbunching that can significantly degrade the beam quality [3, 4, 5, 6]. Recently, Saldin *et al.* pointed out that the longitudinal space charge (LSC) field can be the main effect driving the microbunching instability in the TESLA test facility (TTF) (phase 2) linac [7]. In addition, significant LSC-induced energy modulation in the DUV-FEL linac has been experimentally characterized using an rf zero-phasing method [8]. Because the microbunching instability is very sensitive to the uncorrelated (local) energy spread of the electron beam, increasing it within the FEL tolerance can provide strong Landau damping against the instability. In this paper, we study the suppression of the microbunching instability driven by LSC, CSR, and linac wakefields in the linac coherent light source (LCLS) using an effective laser heater.

MICROBUNCHING INSTABILITY

The mechanism for microbunching instability is similar to that in a klystron amplifier [4]. A high-brightness electron beam with a small amount of longitudinal density modulation can create self-fields that lead to beam energy modulation. Since a magnetic bunch compressor (usually a chicane) introduces path length dependence on energy, the induced energy modulation is then converted to additional density modulation that can be much larger than the initial density modulation. This amplification process (the gain in microbunching) is accompanied by a growth of energy modulation and a possible growth of emittance if significant energy modulation is induced in a dispersive region such as the chicane. Thus, the instability can be harmful to FEL performance, which depends critically on the high quality of the electron beam.

The initial electron density modulation is most likely caused by the intensity fluctuation on the drive laser that produces the electron beam from the photocathode. The electrons repel each other in the higher density regions and initiate the space charge oscillation between density and energy modulations in the low-energy section of a photoin-

jector. As a result, the initial density modulation at the injector end may be reduced by a factor of a few, while noticeable energy modulation can be accumulated in the injector [9]. Start-to-end simulations including the injector modulation dynamics are carried out to specify the tolerable drive-laser modulation level [10]. In this paper, we neglect the injector modulation dynamics for simplicity and focus on the amplification of only small density modulations starting from the injector end.

At the end of the LCLS photoinjector (at 135 MeV in Fig. 1), the electrons are too relativistic to have any relative longitudinal motion in the linac. Thus, the electron density modulation is frozen while the energy modulation is accumulated in the linac. After a bunch compressor, the gain in density modulation for a Gaussian energy distribution is [4]

$$G_0 \approx \frac{I_0}{\gamma I_A} \left| k_f R_{56} \int_0^L ds \frac{4\pi Z(k_0; s)}{Z_0} \right| e^{-k_f^2 R_{56}^2 \sigma_\delta^2 / 2} \quad (1)$$

where I_0 and I_A (≈ 17 kA) are the initial and Alfvén current, $k_0 = 2\pi/\lambda_0$ and $k_f = k_0/|1 + hR_{56}|$ are the initial and compressed modulation wavenumber, h is the (linear) chirp, R_{56} is the momentum compaction of the chicane, L is the linac length, $Z_0 = 377 \Omega$ is the free space impedance, and σ_δ is the relative uncorrelated energy spread prior to the chicane. The longitudinal impedance $Z(k_0)$ per unit length includes geometric wakefields and LSC given by [11, 12]

$$Z_{\text{LSC}}(k_0) = \frac{iZ_0}{\pi k_0 r_b^2} \left[1 - \frac{k_0 r_b}{\gamma} K_1 \left(\frac{k_0 r_b}{\gamma} \right) \right], \quad (2)$$

where r_b is the radius of the uniform cross section and is approximately the sum of rms beam sizes in both transverse planes for a Gaussian or parabolic cross section, and K_1 is the modified Bessel function. Effects of the vacuum chamber are ignored for these very short modulation wavelengths. We have also neglected a small transverse variation of the LSC field that can contribute to a slight increase of the local energy spread. The LSC impedance is implemented in the numerical tracking code *elegant* [13].

Both photoinjector simulations and measurements [14] show an uncorrelated energy spread about 3 keV (rms) at ≥ 1 nC charge, yielding $\sigma_\delta = 1.2 \times 10^{-5}$ at the BC1 energy of 250 MeV. With such a small intrinsic energy spread, the peak gain including CSR amplification [5, 6] after BC1 can be on the order of 100. With two bunch compressors designed for the LCLS, the total gain after BC2 can be $\sim 10^4$ and may even amplify shot-noise fluctuations [15].

The very large gain in density modulation at these short wavelengths can be suppressed by increasing the uncorre-

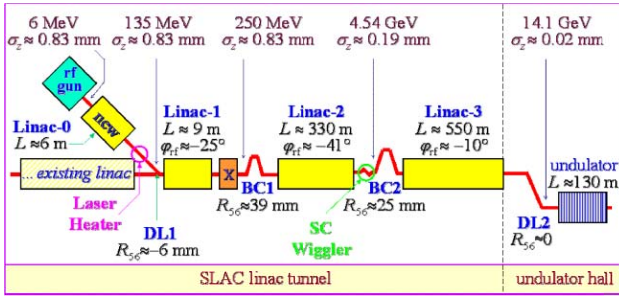


Figure 1: LCLS accelerator system layout with a laser heater at 135 MeV or a SC wiggler at 4.5 GeV.

lated energy spread of the electron beam. Note the uncorrelated energy spread after compression and acceleration is less than 1×10^{-5} at the undulator (14 GeV). Since the FEL parameter $\rho \approx 5 \times 10^{-4}$ for the LCLS when the fundamental radiation wavelength is 1.5 \AA , a factor of 10 to 15 increase in uncorrelated energy spread has a rather minimal impact on the FEL performance. Taking into account that quantum fluctuations of spontaneous radiation in a 130-m undulator can increase the rms energy spread to $\sim 2 \times 10^{-4}$ [1], the average power gain length is almost independent of the slice (over FEL slippage length) energy spread σ_{δ_f} up to 1×10^{-4} . However, for $\sigma_{\delta_f} > 1 \times 10^{-4}$, the FEL gain length and hence the saturation length starts to increase much faster. Thus, the tolerable rms energy spread at the undulator entrance is about 1×10^{-4} or 1.4 MeV.

LASER HEATER

The microbunching instability is predominantly driven by LSC at low-energy section of the linac ($< 1 \text{ GeV}$) and is not effectively suppressed by a superconducting wiggler that increases the uncorrelated energy spread at BC2 (at 4.5 GeV as shown in Fig. 1) [15]. At energies less than about 1 GeV, uncorrelated energy spread cannot be easily increased by quantum fluctuations of synchrotron radiation. Nevertheless, resonant laser-electron interaction in a short undulator induces rapid energy modulation at the optical frequency, which can be used as an effective energy spread for beam “heating” [7, 16].

Suppose a Gaussian laser beam co-propagates with a round electron beam at the energy $\gamma_0 mc^2$ ($= 135 \text{ MeV}$) in a planar undulator of length L_u , which is short compared to both the Rayleigh length Z_R of the laser and the beta functions $\beta_{x,y}$ of the electrons. The energy modulation amplitude of the resonant FEL interaction is

$$\Delta\gamma_L(r) = \sqrt{\frac{P_L}{P_0}} \frac{K[\text{JJ}]L_u}{\gamma_0\sigma_r} \exp\left(-\frac{r^2}{4\sigma_r^2}\right), \quad (3)$$

where P_L is the peak laser power, $P_0 = I_A mc^2/e \approx 8.7 \text{ GW}$, K is the undulator parameter, $[\text{JJ}]$ is the Bessel-function factor, r is the radial position of the electron, and σ_r is the rms laser spot size. Table 1 lists the main laser heater parameters under design at the end of the LCLS photoinjector (see Fig. 1). Two sets of laser spot size and

Table 1: Main parameters for the LCLS laser heater.

Parameter	Value
electron energy $\gamma_0 mc^2$	135 MeV
average beta function $\beta_{x,y}$	10 m
transverse rms e-beam size $\sigma_{x,y}$	190 μm
undulator period λ_u	0.05 m
undulator parameter K	1.5
undulator length L_u	0.5 m
laser wavelength λ_L	765 nm
laser rms spot size σ_r	175 μm (1.5 mm)
laser peak power P_L	1.2 MW (37 MW)
Rayleigh range Z_R	0.5 m (37 m)
max. energy mod. $\Delta\gamma_L(0)mc^2$	80 keV (55 keV)

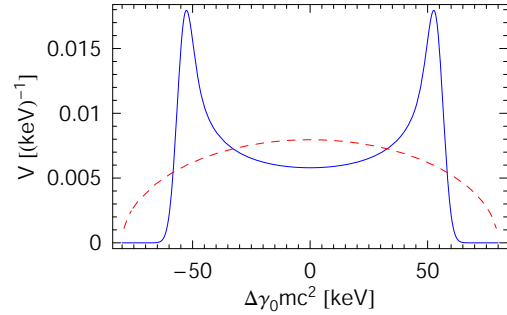


Figure 2: Electron energy distribution after the laser heater for a large laser spot (blue) and for a matched laser spot (red). The laser powers are given in Table 1 so that the rms energy spread $\approx 40 \text{ keV}$ for both distributions.

peak power are considered, both of which increase the rms energy spread from 3 keV to about 40 keV. After a total compression factor of about 30, the slice rms energy spread should be about 1.2 MeV or $\sigma_{\delta_f} \approx 0.9 \times 10^{-4}$ at the undulator entrance (at 14 GeV) in the absence of impedance effects. The necessary laser power (37 MW) for the large laser spot size ($\sigma_r = 1.5 \text{ mm}$) is still a small fraction of the available power of the Ti-Sapphire laser that drives the photocathode rf gun and hence can be extracted from it.

Assuming initially Gaussian distributions in energy and in transverse coordinates, we obtain the modified energy distribution after the laser heater as shown in Fig. 2 for $\sigma_r \gg \sigma_x$ (when the laser spot size is much larger than the electron beam size) and $\sigma_r \approx \sigma_x$ (when the laser spot size is matched to the e-beam size). A large laser spot size may be useful to establish the initial laser-electron interaction. However, the resulting energy modulation amplitude is almost the same for all electrons, and the energy profile is a double-horn distribution (the blue curve in Fig. 2). The two sharp spikes at $\Delta\gamma_0 \approx \pm\Delta\gamma_L(0)$ act like two separate cold beams that do not contribute much to suppressing the instability. For $\sigma_r \approx \sigma_x$, the off-axis electrons experience smaller modulation with smaller laser field than the on-axis ones (see Eq. (3)). As a result, the “heating” is more uniform in terms of the energy distribution (the red curve in Fig. 2), and we expect better Landau damping. The gain in Eq. (1) is reduced by a suppression factor

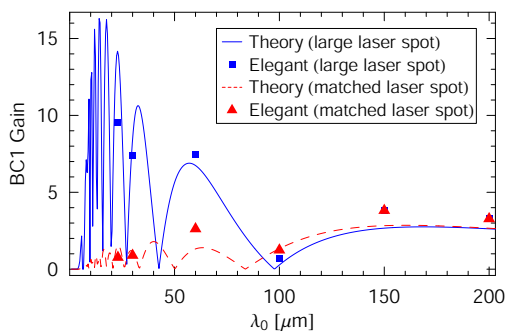


Figure 3: Microbunching gain after BC1 as a function of the initial modulation wavelength λ_0 for a laser heater with a large laser spot (blue) and with a matched laser spot (red).

$S_L(k_f R_{56} \Delta\gamma_L(0)/\gamma, \sigma_r/\sigma_x)$ [15], where

$$S_L(A, B) = \begin{cases} J_0(A), & B \gg 1, \\ \frac{2J_1(A)}{A}, & B = 1. \end{cases} \quad (4)$$

For $|A| = |k_f R_{56} \Delta\gamma_L(0)/\gamma| \gg 1$, the Bessel functions $J_{0,1}(A) \sim |A|^{-1/2}$. Thus, a laser heater with a large laser spot size ($B \gg 1$) has $S_L \sim |A|^{-1/2}$ and suppresses the gain weakly, while a laser heater with a matched spot size ($B = 1$) has $S_L \sim |A|^{-3/2}$ and is more effective at smearing the instability at short wavelengths.

Figure 3 shows that the BC1 gain computed from the linear theory agrees reasonably with *elegant* simulations using two sets of laser spot size and peak power given in Table 1. The theoretical gain after both compressors at short wavelengths ($\lambda_0 \leq 60 \mu\text{m}$) can still be very high (~ 100) for a laser heater with a large spot size because of its ineffective Landau damping at these wavelengths. Starting with 1% initial density modulation, *elegant* simulations show reduced gain at these very short wavelengths as the density modulation after BC2 is not sinusoidal, but the slice energy spread can still increase as a result of the distorted longitudinal phase space (see Fig. 4). Figure 5 shows the slice energy spread of the bunch core at the undulator entrance without a laser heater and in presence of a laser heater with two different spot sizes. Thus, a laser heater with a large laser spot allows the growth of short-wavelength modulations that increases the slice energy spread at the undulator entrance, while a laser heater with a matched laser spot effectively suppresses the instability and does not change the slice energy spread above the design goal (about 1×10^{-4}).

Finally, the laser heater can be embedded in a weak chicane ($R_{56} \approx 3 \text{ mm}$) to allow convenient laser-electron interaction with no crossing angle and to provide a useful temporal washing effect that completely smears the laser-induced 800-nm energy modulation [15]. The implementation of the laser heater in the LCLS photoinjector beam line is described elsewhere [17] in these proceedings.

REFERENCES

- [1] LCLS CDR, SLAC-R-593, SLAC (2002).
- [2] TESLA XFEL, TESLA FEL 2002-09, DESY (2002).

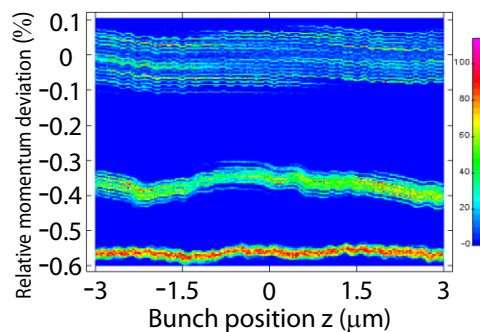


Figure 4: Central portion of the longitudinal phase space without a laser heater (upper), in presence of a laser heater with $\sigma_r = 1.5 \text{ mm}$ (middle) and with $\sigma_r = 175 \mu\text{m}$ (lower) at the undulator entrance. Curves offset vertically for clarity. Simulations are seeded with 1% initial density modulation at $\lambda_0 = 30 \mu\text{m}$.

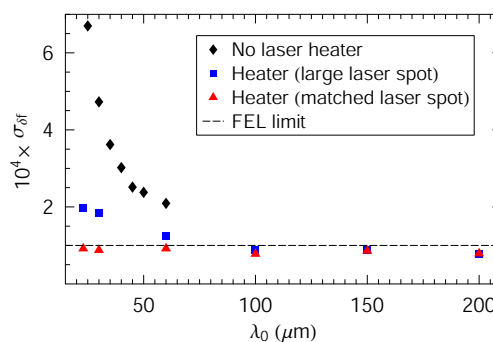


Figure 5: Slice rms energy spread σ_{δ_f} at the undulator entrance at 14 GeV for 1% initial density modulation without a laser heater (black), in presence of a laser heater with a large spot size (blue) and with a matched spot size (red).

- [3] M. Borland et al., Nucl. Instrum. Methods A **483**, 268 (2002).
- [4] E. Saldin, E. Schneidmiller, and M. Yurkov, Nucl. Instrum. Methods A **490**, 1 (2002).
- [5] S. Heifets, G. Stupakov, and S. Krinsky, Phys. Rev. ST Accel. Beams **5**, 064401 (2002).
- [6] Z. Huang and K.-J. Kim, Phys. Rev. ST Accel. Beams **5**, 074401 (2002).
- [7] E. Saldin, E. Schneidmiller, and M. Yurkov, TESLA-FEL-2003-02, DESY (2003).
- [8] T. Shafiq and Z. Huang, BNL-71491, BNL (2003).
- [9] C. Limborg et al., in EPAC2004 (2004).
- [10] J. Wu et al., SLAC-PUB-10430, in LINAC2004 (2004).
- [11] J. Rosenzweig et al., TESLA-FEL-96-15, DESY (1996).
- [12] Z. Huang and T. Shafiq, SLAC-PUB-9788, SLAC (2003).
- [13] M. Borland, APS LS-287, ANL (2000).
- [14] M. Hüning and H. Schlarb, in PAC2003, 2074 (2003).
- [15] Z. Huang et al., SLAC-PUB-10334, accepted in PRST-AB (2004).
- [16] J. Galayda, private communication.
- [17] R. Carr et al., in EPAC2004 (2004).